Materials Horizons

A Transparent *p*-Type Semiconductor Designed via a Polarizability-Enhanced Strongly Correlated Insulator Oxide Matrix

Journal:	*Materials Horizons*
Manuscript ID	MH-COM-07-2024-000985.R1
Article Type:	Communication
Date Submitted by the Author:	06-Sep-2024

Complete List of Authors:	Lee, Seung Yong; Yonsei University Kim, Inseo; Kunsan National University Kim, Hyun Jae; Korea Electronics Technology Institute, Display Research Center; Yonsei University Sim, Sangjun; Kunsan National University Lee, Jae Hoon; Kunsan National University Yun, Sora; Kunsan National University Bang, Joonho; Gyeongsang National University, School of Materials Science and Engineering Park, Kyoungwon; Korea Electronics Technology Institute, Display research center Han, Chul jong; Korea Electronics Technology Institute, Kim, Hyun-Min ; Hongik University, Materials Science and Engineering Yang, Heesun; Hongik University, Materials Science and Engineering Kim, Bongjae; Kyungbuk National University Im, Seongil; Yonsei University, Institute of physics and applied physics Facchetti, Antonio; Georgia Institute of Technology Oh, Min Suk; Korea Electronics Technology Institute, Display Research Center Lee, Kyu Hyoung; Yonsei University, Lee, Kimoon; Kunsan National University, Department of Physics

COMMUNICATION

A Transparent *p*-Type Semiconductor Designed via a Polarizability-Enhanced Strongly Correlated Insulator Oxide Matrix

Received 00th January 20xx,
Accepted 00th January 20xx

DOI: 10.1039/x0xx00000x

Seung Yong Lee[a,b†], Inseo Kim[c†], Hyun Jae Kim[a,d†], Sangjun Sim[c], Jae-Hoon Lee,[c,e], Sora Yun[c], Joonho Bang[f], Kyoung Won Park[d], Chul Jong Han[d], Hyun-Min Kim[g], Heesun Yang[g], Bongjae Kim[h], Seongil Im[i], Antonio Facchetti*[j], Min Suk Oh*[d], Kyu Hyoung Lee[a]*, and Kimoon Lee[c,k]*

Electron-transporting transparent conducting oxides (TCOs) are a commercial reality, however, hole-transporting counterparts are far more challenging because of limited material design. Here, we propose a strategy for enhancing the hole conductivity without deterioratinhg the band gap (E_g) and workfunction (Φ) by Cu incorporation in a strongly correlated $NiWO_4$ insulator. The optimal Cu-doped $NiWO_4$ ($Cu_{0.185}Ni_{0.815}WO_4$) exhibits a resistivity reduction of ~10^9 times versus $NiWO_4$ as well as band-like charge transport with a hole mobility approaching 7 $cm^2/V{\cdot}s$ at 200 K, a deep Φ of 5.77 eV, and E_g of 2.8 eV. Experimental and theoretical data reveal that the strength of the electron correlation in $NiWO_4$ is not frustrated by Cu incorporation, while the promoted polarizability weakens electron-phonon coupling favouring large polaron appearance. Quantum dot light-emitting and oxide *p/n* junction devices incorporating $Cu_{0.185}Ni_{0.815}WO_4$ exhibit remarkable performances, demonstrating that our approach can be deployed to discover new *p*-type TCOs.

[a] *Department of Materials Science and Engineering, Yonsei University, Seoul 03722, Republic of Korea.*
[b] *KIURI Institute, Yonsei University, Seoul 03722, Republic of Korea.*
[c] *Department of Physics, Kunsan National University, Gunsan 54150, Republic of Korea.*
[d] *Display Research Center, Korea Electronics Technology Institute (KETI), Seongnam 13509, Republic of Korea.*
[e] *Global Infra Technology, Samsung Electronics, Yongin 17113, Republic of Korea.*
[f] *School of Materials Science & Engineering, Gyeongsang National University, Jinju 52828, Republic of Korea.*
[g] *Department of Materials Science and Engineering, Hongik University, Seoul 04066, Republic of Korea.*
[h] *Department of Physics, Kyungbuk National University, Daegu 41566, Republic of Korea.*
[i] *Department of Physics, Van der Waals Materials Research Center, Yonsei University, Seoul 03722, Republic of Korea.*
[j] *School of Materials Science and Engineering, Georgia Institute of Technology, Atlanta, GA 30332, USA.*
[k] *The Institute of Basic Science, Kunsan National University, Gunsan 54150, Republic of Korea.*
† These authors contributed equally to this work.
Supplementary Information available: [details of any supplementary information available should be included here]. See DOI: 10.1039/x0xx00000x

New Concepts

In the present work, we report a novel strategy for developing an outstanding transparent *p*-type (semi)conducting oxide (*p*-TCO), exhibiting the deepest work function as well as a wide band gap to date among *p*-TCOs by engineering the polarizability of a strongly correlated oxide matrix through a conventional chemical route of atomic substitution. By substituting Cu into strongly correlated $NiWO_4$, we successfully attain for the composition $Cu_{0.185}Ni_{0.815}WO_4$ a high hole carrier mobility approaching 7 cm^2/Vs at 200 K, a deep work function of 5.77 eV, and a large optical gap E_g of 2.8 eV (even 3.8 eV in direct E_g). Equally important this new oxide material composition exhibits a band-like large polaronic conduction achieved without frustrating Ni *d–d* electron correlation strength, which is associated with the deepest-lying delocalized valence band maximum state in metal oxides, to the best of our knowledges. As a practical application, we also demonstrate that the best composition functions as an efficient hole transporting layer in a quantum dot light-emitting diode as well as oxide *p/n* junction rectifier, enabling high luminescence/efficiency and on/off switching ratio, respectively.

Introduction

Several modern (opto)electronic devices utilize the complementary charge transport in semiconductors for optimal operation.[1-8] Manipulating their conduction and transition with opposite polarities at a distinct energetic potential has been a great technological issue covering systems ranging from traditional Si-based circuitries to nanoscale systems beyond the quantum limit.[1-8] For instance, complementary metal-oxide-semiconductor-type (CMOS-type) electronic devices operate by simultaneous opposite switching behaviour based on rationally connected *n*- and *p*-type transistors in which electrons and holes serve as the majority current deliverer, respectively.[1-3] Optoelectronic devices, such as photodetectors/emitters and photovoltaic cells, also employ excitation/recombination processes between electrons and holes lying at distant energy

levels.[5-8] Transparent conducting oxides (TCOs) are (semi)conductors that are transparent in the visible spectrum, and can transport both electrons and holes with the former widely commercialized.[3,8-14] In particular, their optical transparency and large exciton binding energy even over large electrical conductivity (σ) variations have paved the way for several applications from defrosting to ultra-high definition (UHD) displays and smart functional windows.[3,8-13] Despite such advances, improvements of TCO-based devices remain hindered by the imbalanced performance between *n*- and *p*-type TCOs, thus a strategy to balance their transport is critical to realize new type of devices.[3,9,14]

The main obstacle inhibiting charge transport balance in TCOs is the trade-off relation between hole carrier mobility (μ_H) and the optical band gap (E_g).[8-11,14] Because a deep-lying valence band maximum (VBM) state across a large E_g typically results to a narrow bandwidth/poor orbital overlap and localized hole transport when approaching core levels,[8-11,14-18] the realization of *p*-type TCOs exhibiting respectable μ_H, wide E_g, as well as deep work function (Φ) is far more challenging than for *n*-type ones. In addition, the optical transparent critically relates to E_g that could be narrowed with elevating VBM level position, deep Φ is favoured to secure wide E_g. To overcome such a limitation, several studies have explored Cu- or Sn-based oxides whose VBM partially comprises more diffused metal *d* and/or *s*-orbitals.[3,9,14,15] However, because of the raised VBM energy, these materials exhibit a E_g and Φ smaller than ~2 and ~5 eV, respectively, thus they are poorly transparent and inefficient for hole injection/extraction.[3,9,14,15] Recent studies suggest that strongly correlated metallic oxides could be a new entry for *p*-type TCO candidates.[19,20] From the large effective mass under strong electron-electron interactions, the free carrier reflection edge shifts outside the visible energy range, thus visible transparency can be attained even under high hole carrier concentrations greater than ~10^{21} cm^{-3}.[19,20] However, such a metallic nature inherently leads to a high absorption coefficient as well as screens the electric field in field-effect transistor (FET) devices, therefore only very thin layers (<10 nm) can be utilized to secure optical transparency and prevent their use as FET-active channel layers.[19,20]

Recently, we proposed a compositional tuning approach for enhancing hole conductivity while maintaining a wide band gap (E_g) by utilizing a Mott-Hubbard insulator system under strong electron correlation.[21] By partial substitution of Ni with Cu in NiO, the polaron hopping efficiency was improved without much suppression of the correlation strength. However, this material showed a very low μ_H of 0.007 $cm^2/V{\cdot}s$, and charge transport remains dominated by the small polaron hopping (SPH) limit. Inspired by the previous study, we hypothesized that a less correlated system, possibly alleviating polaronic distortion, could lead to greater hole mobility and band-like charge transport while retaining a deep-lying VBM and transparency. In this study, we report ternary (monoclinic) $NiWO_4$ with lower symmetry than binary (cubic) NiO as the matrix material to prove this concept. By synthesizing Cu-substituted $NiWO_4$ ($Ni_{1-x}Cu_xWO_4$, $0.00 \leq x \leq 0.20$), a considerable increase in the electrical conductivity by ~10^9 times for x = 0.20, compared to that of intrinsic $NiWO_4$, was measured. From electrical, optical, magnetic, and theoretical characterizations, Cu substitution in $NiWO_4$ gives rise to high μ_H approaching 7 $cm^2/V{\cdot}s$ at 200 K, exhibiting nonthermally activated behaviour without much variation both in E_g and the magnetic transition temperature. This result demonstrates the emergence of large polaronic hole conduction under a sustained correlation strength. The excellent E_g and Φ values larger than 2.7 and 5.56 eV, respectively, even at a high Cu content of 0.20 demonstrate that such delocalized hole conduction occurs through a very deep-lying VBM and a wide E_g, which is essential for optimal *p*-type TCO. This newly developed $Ni_{1-x}Cu_xWO_4$ functions as an efficient hole transporting layer (HTL) in both quantum dot light-emitting diodes (QD-LEDs) and oxide-based *p*/*n* junction rectifiers, further corroborating the potential of this *p*-type TCO for practical applications.

Methods

Materials synthesis and characterization

Polycrystalline $Ni_{1-x}Cu_xWO_4$ were synthesized by a solid-state reaction process. After mixing stoichiometric amounts of NiO, CuO, and WO_3 powders (99.998%, 99.995% and 99.998% purity, respectively) in an agate mortar, the mixtures were annealed at 950 ℃ for 24 h. The annealed powders were pulverized, then pressed into pellet form, followed by heating at 950 ℃ for 24 h. By repeating the same pulverizing/pressing and annealing processes two more times, homogeneous and single phase $Ni_{1-x}Cu_xWO_4$ samples ($0.00 \leq x \leq 0.20$) could be finally obtained. The crystalline structures of synthesized samples were analysed by XRD measurement. (MiniFlex 600, Rigaku) Compositional analysis was performed by inductively coupled plasma mass spectroscopy (ICP-MS). (7900 ICP-MS, Agilent) The vibrational modes of $Ni_{1-x}Cu_xWO_4$ samples were characterized by Raman spectroscopy with 532 nm wavelength excitation. (RAMANtouch, nanophoton) The electrical resistivity in high T region (300 − 570 K) was measured by 4-point-probe method using semiconductor parameter analyser. (4200-SCS, Keithley) Hall-effect measurement in low T region (160 − 260 K) was performed by utilizing high-precision current source, nanovolt meter, and Hall-effect card (6220, 2182A, and 3756, Keithley, respectively) equipped with a cryogen-free cryostat and a 1.2 T electro-magnet. (Co-designed by I.V SOLUTION and Sungwoo Instruments Inc.) For the electrical measurement, we applied Ag paste on the square-cutting densified pellet (the inset photo in figure 1c) with Hall-bar geometry, then wired to the external instruments. Optical absorption spectra and magnetic properties were investigated by spectroscopic ellipsometer (M-2000, JA Woollam) and magnetic property measurement system (MPMS, Quantum Design), respectively. Ultraviolet photoemission spectroscopy (UPS) measurements were carried out by using a hemispherical analyser with a He I (21.2 eV) source. (AXIS Supra$^+$, KRATOS Analytical) For insulating surface nature of $Ni_{1-x}Cu_xWO_4$, the charge neutralization system was applied onto the ion-etched surface under a sample bias of -10 V to obtain the true cut-off of the secondary electron emission.

Electrical permittivity was measured by impedance analyser (HP4284, Agilent) with varying frequency from 1 kHz to 1 MHz at 300 K.

Density functional theory (DFT) calculations

All DFT calculations were performed using the projector augmented wave (PAW) method implemented in the vienna *ab initio* simulation package (VASP) code.[22,23] Starting from the experimental input, the lattice parameters and internal coordinates of the atoms were fully relaxed with a force criteria of 1 meV/Å. We employed the generalized gradient approximation (GGA) exchange-correlation potential with plane-wave energy cutoff of 500 eV.[24] It was confirmed that the magnetic ground state was well reproduced by total energy calculation. (See supporting Fig. S1.) To study of the substitution effect, twice larger supercell was constructed, which includes 8 f.u. and one Ni out of eight was substituted with Cu to simulate the $x = 0.125$ substitution case. $4 \times 8 \times 8$ and $4 \times 8 \times 4$ of *k*-point meshes were sampled for pristine and Cu-substituted $NiWO_4$, respectively. To treat the correlation of transition metal *d*-electrons, $U = 6$ eV and 8 eV were used for Ni 3*d* and Cu 3*d* with Dudarev scheme within DFT+*U* approach.[25-27]

QD-LED device fabrication and characterization

To fabricate QD-LED devices, indium tin oxide (ITO, 150 nm) coated glass substrates (25×25 mm^2) were patterned by the conventional photolithography method and wet etching process after cleaning with acetone, methanol, and isopropyl alcohol (IPA) by ultrasonic cleaner. Then the substrates were rinsed with deionized water and blown with N_2. The patterned ITO glass substrates were treated by O_2 plasma at 150 W for 300 sec, then 1.25 wt.% tungsten oxide nanoparticles (~30 nm, Sigma-Aldrich) in 2-propanol were spin-coated on the ITO glasses at 500 rpm for 5 sec and 5500 rpm for 30 sec. To remove the residual solvent, they were baked at 100 ℃ for 30 min. The 30 nm-thick $Ni_{0.815}Cu_{0.185}WO_4$ layers as hole transport layer (HTL) were deposited by RF magnetron sputtering process (10 mTorr, 100 W) using sintered target with the same stoichiometry through shadow mask in Ar ambient at RT, (deposition rate was 8.3 nm/min) followed by rapid thermal annealing process at 300 ℃ for 10 min in O_2 ambient. (3×10^2 Torr) As the emission layer, CdSe-based QDs of 10 mg/ml in toluene were spin-coated on the $Ni_{0.815}Cu_{0.185}WO_4$-deposited substrates at 500 rpm for 2 sec and 2000 rpm for 20 sec. (Detailed synthetic process for QDs is described in the electronic supplementary information (ESI).) After QD coating, the substrates were treated at 100 ℃ for 10 min on a hot plate in the glove box. As electron transport layer (ETL) and electron injection layer (EIL), we deposited TPBi (1,3,5-Tris(1-phenyl-1Hbenzimidazol-2-yl)benzene, Luminescence Technology Corp.) and lithium fluoride (LiF), respectively, by thermal evaporation. For the cathode, 80 nm-thick Al was deposited through a shadow mask by thermal evaporation. The fabricated devices were encapsulated by the encapsulation glass using UV sealant in the glove box with nitrogen. The device structure was measured by HR-TEM. (JEM-2100F, JEOL) Current density-voltage-luminance (*J-V-L*) characteristics and electroluminescence (EL) spectra of QD-LEDs were measured by spectroradiometer (CS-2000A, Konica Minolta) and Keithley 2400 Source Measure Unit.

Oxide *p/n* junction rectifying device fabrication and characterization

To fabricate *p*-$Ni_{0.815}Cu_{0.185}WO_4$/*n*-IGZO junction rectifying device, indium tin oxide (ITO, 150 nm) coated glass substrates (25×25 mm^2) were cleaned with acetone, methanol, and isopropyl alcohol (IPA) by ultrasonic cleaner. Then the substrates were rinsed with deionized water and blown with N_2. The 100 nm-thick IGZO film was RF sputtered on the cleaned ITO glasses (3 mTorr, 100 W) under working pressure of Ar/O_2 condition ($Ar : O_2 = 10:1$), (deposition rate was 1.4 nm/min) followed by rapid thermal annealing process at 300 °C for 10 min in air ambient. The same 100 nm-thick $Ni_{0.815}Cu_{0.185}WO_4$ layer were deposited also by RF magnetron sputtering process (10 mTorr, 100 W) using the same sintered target with HTL in QD-LED in $Ar : O_2 = 2:1$ ambient at RT, followed by rapid thermal annealing process at 300 ℃ for 10 min in O_2 ambient. (3×10^2 Torr) For the top-contact ohmic electrode, 100 nm-thick Au was deposited through a shadow mask by thermal evaporation. Static current-voltage (*I-V*) characteristics were measured using semiconductor parameter analyzer (4200-SCS, Keithley) in dark and air ambient at RT. Dynamic rectifying characteristics of fabricate *p*-$Ni_{0.815}Cu_{0.185}WO_4$/*n*-IGZO junction rectifier under various AC conditions were measured using a function generator (AFG 3022B, Tektronix) and an oscilloscope (TDS 2014B, Tektronix) with a serial R_L of 100 kΩ at RT.

Results & discussion

Materials synthesis and characterization

For sample preparation, we synthesized $Ni_{1-x}Cu_xWO_4$ with different *x* contents from 0 to 0.25 through the conventional solid-state reaction process (see details in Methods). Figure 1a illustrates the crystal structure of $Ni_{1-x}Cu_xWO_4$ for different *x* values obtained by Rietveld refinement of the powder X-ray diffraction (PXRD) measurements (see supporting Figs. S2, S3 and Table S1 for details). Regardless of the *x* value, all samples show a monoclinic structure with a space group of *P*12/*c*1, belonging to a relatively low symmetry group compared to cubic binary NiO.[21] PXRD shows no observable impurity except for the sample with $x = 0.25$, as marked by the asterisk in Fig. S2. As shown in Fig. 1b, the unit cell volume linearly increases with increasing *x*, mainly originating from the *b*-axis expansion. Accompanied by the quantitative *x* values plotted in Fig. 1c (Table S2), this result demonstrates that Cu homogeneously substitutes Ni forming a solid solution, a data consistent with the Rietveld refinement results and the Vegard's rule.[21] Fig. 1d shows the Raman spectra in selected regions for $Ni_{1-x}Cu_xWO_4$ samples (for full-range spectra see Fig. S4). The Raman peak ~370 cm^{-1} originates from symmetric A_{1g} vibration of [NiO_6] octahedra, while those ~700 and ~900 cm^{-1} are assigned as W-O-W and [WO_6] octahedra symmetric vibration modes, respectively.[28] (see Fig. 1d) Note that the vibrational energy is proportional to $\sqrt{k/\mu}$, where *k* and μ are the spring constant and the reduced mass, respectively, resulting in the systematic

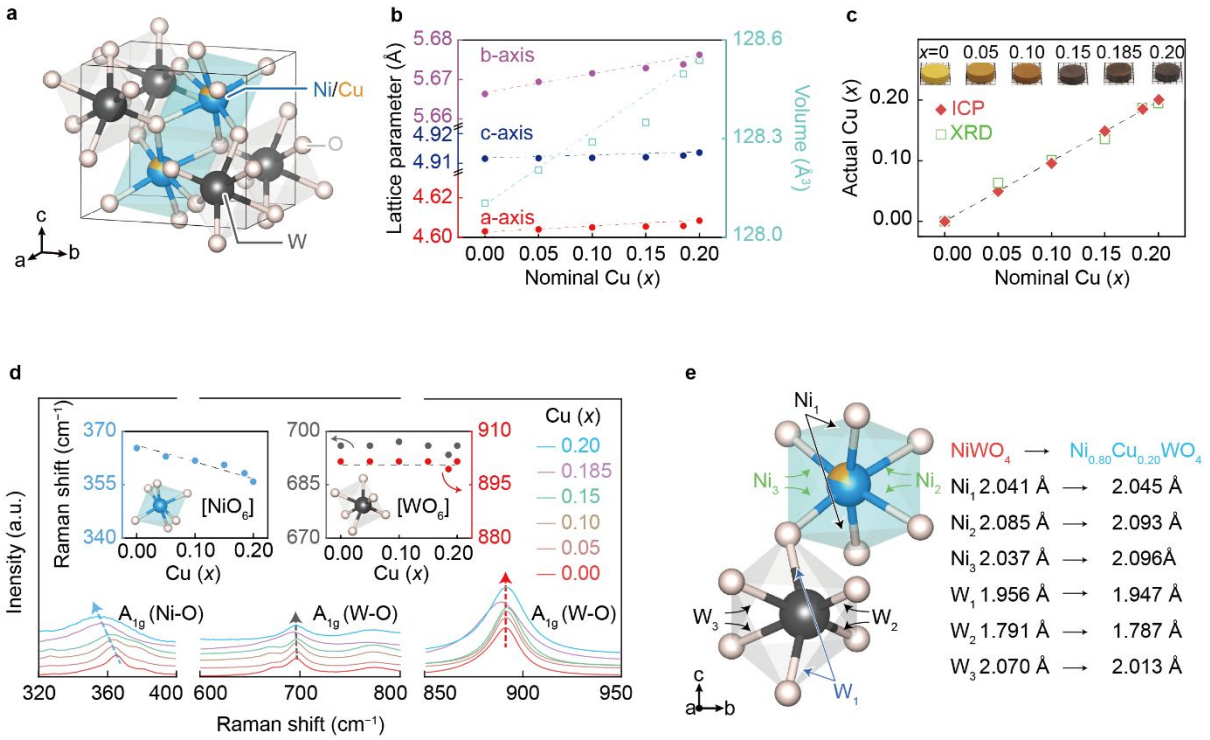

Figure 1. Characterization of $Ni_{1-x}Cu_xWO_4$ samples. (a) Crystal structure of $Ni_{1-x}Cu_xWO_4$ ($0.00 \le x \le 0.20$) obtained by the Rietveld refinement of PXRD patterns. (b) Lattice parameters and unit cell volume from PXRD data as a function of *x*. (c) Atomic composition of Cu-substitution contents, *x*, characterized by ICP-MS and Rietveld analysis. The inset photo displays the colours of synthesized $Ni_{1-x}Cu_xWO_4$ samples with different *x* values. (d) Raman spectra from $Ni_{1-x}Cu_xWO_4$ samples. The characteristic peak positions for Ni-O and W-O vibrational modes as a function of *x* are plotted in the inset. (e) The local structure of $[NiO_6]$ and the nearest $[WO_6]$ octahedral units. The bond length changes with Cu substitution are also defined.

Raman peak shift associated not only to the change of μ but also to the strain effect in the substitutional solid-solution system.[29] Since the Raman peak associated with $[NiO_6]$ octahedra redshifts with increasing *x*, in contrast to the negligible changes in the $[WO_6]$-associated peaks, this result further demonstrates that Cu substitutes Ni and not W as evidenced by the bond length changes depicted in the local structure of corner-sharing $[NiO_6]$ and its neighbouring $[WO_6]$ (Fig. 1e). Element mapping by scanning electron microscopy (SEM) – energy dispersive X-ray spectroscopy (EDS) also confirms that Cu-substitutions are uniformly distributed through whole sample area. (see Fig. S5)

Charge carrier transport analysis

The electrical properties of $Ni_{1-x}Cu_xWO_4$ samples were measured on densified pellet forms contacting with Ag paste electrodes with a Hall bar geometry (details in Methods). Figure 2a displays the changes in the electrical resistivity (ρ) at 300 K for $Ni_{1-x}Cu_xWO_4$ samples, demonstrating that ρ drastically decreases from 3.69×10^{12} to 3.28×10^{3} Ω·cm as *x* increases. When we measured the temperature (*T*) dependence of ρ from 300 to 570 K, we found that all samples show thermally activated behaviour regardless of *x* as shown in Fig. 2b. Note that a kink at ~400 K for $x = 0$ is possibly due to the mixed conduction at high *T*,[30] however, all samples display a linear relationship in the $\ln(\rho/T)$ versus $1/T$ plot. It demonstrates that the charge transport mechanism in $Ni_{1-x}Cu_xWO_4$ at high *T* (where the electron-phonon interaction is strong) follows the SPH model, resulting in relatively low μ_H values in line with other Ni-based transition metal oxides.[17,18,20,21] However, the slope of the $\ln(\rho/T)$ versus $1/T$ plot decreases as *x* increases (Fig. 2a), confirming that the activation energy (E_a) for SPH conduction is suppressed upon Cu incorporation as also observed in Cu-substituted NiO. Note that the smallest E_a corresponds to a value of 0.16 eV versus 0.24 eV measured for NiO,[21] suggesting that the hopping probability in monoclinic ternary $NiWO_4$ is much improved compared to that in the rigid cubic binary NiO system.

To investigate charge transport details in $Ni_{1-x}Cu_xWO_4$, we performed Hall-effect measurements on the most conductive samples with $x = 0.185$ and 0.20 at low *T* (160 – 260 K), where the phonon-associated interaction is relatively inactive.[17,18,31] Figure 2c-e reports σ, the carrier concentration (*p*), and μ_H as a function of *T*. From Fig. 2c, both samples show similar thermally activated behaviour of σ in the high *T* region. In contrast to the high *T* region, definite Hall voltages with positive values start to be detected in the low *T* region for $x = 0.185$ and 0.20, revealing the *p*-type polarity of $Ni_{1-x}Cu_xWO_4$. Based on the measured Hall voltage with decreasing *T*, we can obtain a log *p* versus $1/T$ plot as shown in Fig. 2d. When we extracted the acceptor ionization energy by extrapolating the Arrhenius relation,[1] values of 0.68 and 0.52 eV are obtained for $x = 0.185$ and 0.20, respectively, indicating the quite far energetic distance between the acceptor level and the VBM for hole carrier generation. From the relation $\sigma = p \cdot e \cdot \mu_H$, where *e* is the elemental charge,[1] the *T*

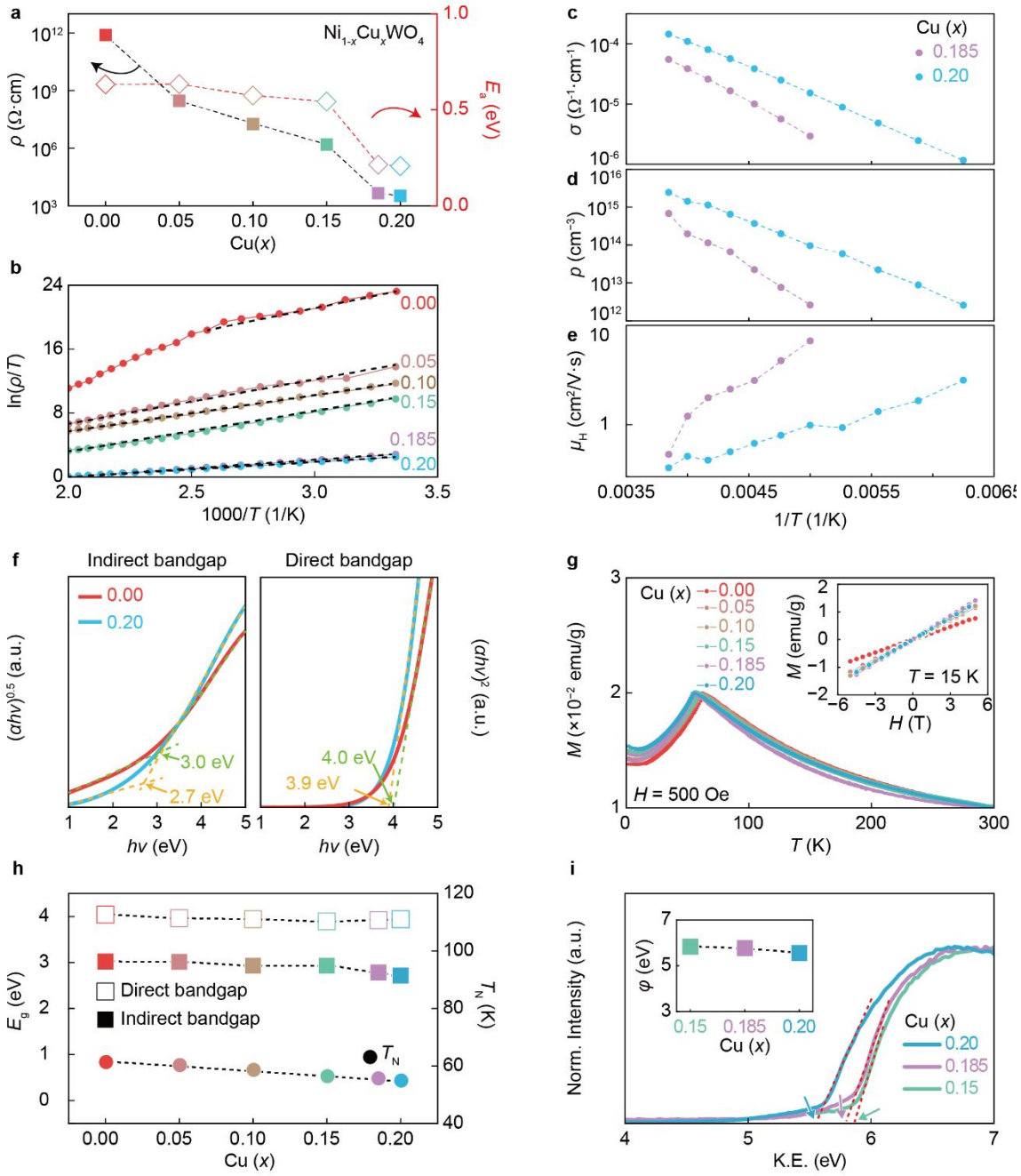

Figure 2. Physical properties of the $Ni_{1-x}Cu_xWO_4$ samples. (a) Changes of ρ and activation energy for small polaron hopping as a function of x in $Ni_{1-x}Cu_xWO_4$. (b) $\ln(\rho/T)$ versus $1/T$ curves from 300 to 570 K for various x. The linear slopes for estimating activation energy is marked by dashed lines. The $1/T$ dependence of (c) σ, (d) p, and (e) μ_H for $Ni_{1-x}Cu_xWO_4$ with x = 0.185 and 0.20 in low T region. (160 – 260 K) (f) Indirect and direct E_g estimation for $Ni_{1-x}Cu_xWO_4$ samples with x = 0.00 and x = 0.20 by fitting optical absorption spectra. (g) M versus T curves measured under H of 500 Oe. M versus H curves measured at 15 K are also shown in the inset. (h) E_g and T_N values with respect to x in $Ni_{1-x}Cu_xWO_4$. (i) Cut-off energy obtained by UPS spectra from secondary electron emission for $Ni_{1-x}Cu_xWO_4$ samples with x = 0.15, 0.185, and 0.20. The inset shows the extracted Φ values with respect to x.

dependence of μ_H can be plotted as displayed in Fig. 2e. Note that μ_H increases, reaching the highest value of 6.98 $cm^2/V{\cdot}s$ (at 200 K for x = 0.185), with decreasing T, overcoming the thermally activated behaviour of both samples. This result strongly evidences the emergence of band-like transport dominated by electron-phonon interactions distinctly different from hopping conduction,[17,18,31] suggesting that Cu substitution in $NiWO_4$ plays a critical role as an μ_H enhancer rather than an acceptor impurity.

Degree of electron correlation relating with band energy level

Figure 2f shows the optical absorption spectra for indirect and direct E_g estimation from $Ni_{1-x}Cu_xWO_4$ samples with x = 0.00 and 0.20. The spectra for other compositions are displayed in Fig.

S6. As shown in Fig. 2f, an indirect transition of 3.0 eV occurs in $NiWO_4$ (x = 0.00), while a slightly suppressed transition of 2.7 eV with x = 0.20 is measured from the $(\alpha h\nu)^{0.5}$ plot, where α and $h\nu$ denote the absorption coefficient and incident optical energy, respectively. Both samples exhibit direct transition values of approximately 4.0 eV as plotted in Fig. 2f. This result is consistent with the Cu-substituted NiO case, supporting that the electron correlation strength, which is expected to be the main origin for E_g formation, is not very frustrated, resulting in an almost constant E_g value even for a high Cu content of 0.20.[21] Such a degree of correlation could also be estimated from the magnetic properties. Figure 2g shows the T dependence of the magnetization (M) for $Ni_{1-x}Cu_xWO_4$ samples. Antiferromagnetic (AFM) ordering occurs near 61 K for intrinsic $NiWO_4$, which is consistent with previous reports.[32] When Cu is introduced, the Neel temperature (T_N) does not change much, with a slight decrease to 55 K even for a high x Cu concentration of 0.20. This result shows that the magnetism of the system is mostly governed by Ni. Together with the result that the magnetic field (H)-dependent M for all the samples shows a linear relationship without any hysteresis (Fig. 2g-inset), the AFM ground states are not changed by introducing Cu.[21] Importantly, E_g and T_N do not change up to a x = 0.20 (Fig. 2h). Assuming a strongly correlated nature of $NiWO_4$ similar to that of AFM NiO, both T_N and E_g critically depend on the exchange-correlation strength, i.e. U/t, where U is the Coulomb potential, and t is the transfer integral between Ni 3d electrons.[33] This result strongly suggests that the strength of the electron correlation in $NiWO_4$ is not frustrated by Cu substitution.

To understand whether such a rigid correlation also operates at the energy band level, UPS measurements were carried out and a comprehensive band schematic is displayed in Fig. S7. As shown in Fig. 2i, the Φ values can be defined by the cut-off energy of the secondary electron emission obtained from the polycrystalline $Ni_{1-x}Cu_xWO_4$ surfaces with x = 0.15, 0.185, and 0.2.[15,34] Plotting Φ with respect to x (Fig. 2i-inset)

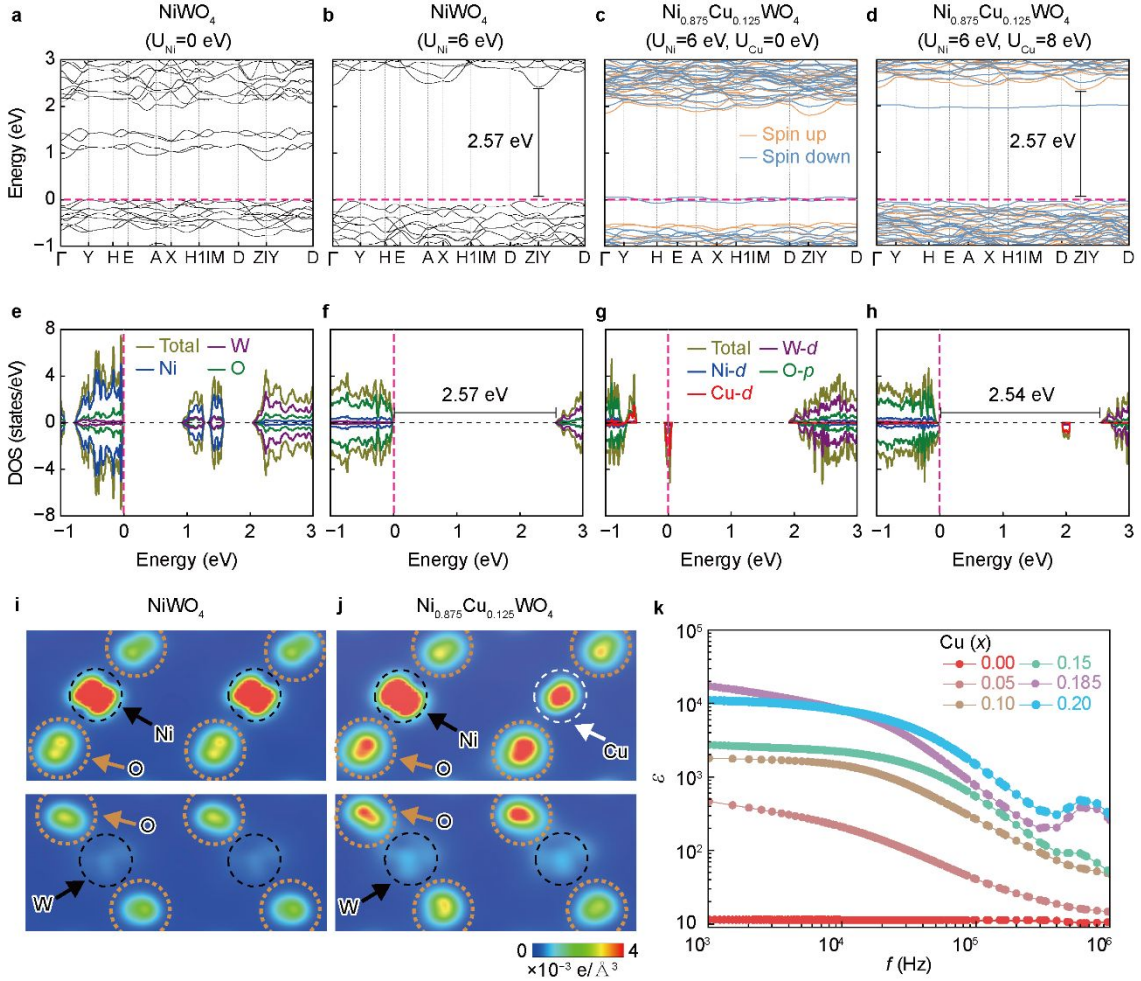

Figure 3. Electron correlation and polarizability study in $NiWO_4$ and $Ni_{1-x}Cu_xWO_4$. Band dispersion calculated from (a) $NiWO_4$ (U_{Ni} = 0 eV), (b) $NiWO_4$ (U_{Ni} = 6 eV), (c) $Ni_{0.875}Cu_{0.125}WO_4$ (U_{Ni} = 6 eV, U_{Cu} = 0 eV), and (d) $Ni_{0.875}Cu_{0.125}WO_4$ (U_{Ni} = 6 eV, U_{Cu} = 8 eV). The respective total/projected DOS of Ni, W, Cu, and O obtained from the (e) $NiWO_4$ (U_{Ni} = 0 eV), (f) $NiWO_4$ (U_{Ni} = 6 eV), (g) $Ni_{0.875}Cu_{0.125}WO_4$ (U_{Ni} = 6 eV, U_{Cu} = 0 eV), and (h) $Ni_{0.875}Cu_{0.125}WO_4$ (U_{Ni} = 6 eV, U_{Cu} = 8 eV). The calculated band gap values are marked in Fig. 3b/3f and 3d/3h for pristine and Cu-substituted $NiWO_4$, respectively. The charge density map on the (013) plane around VBM (E_F – 1 eV to E_F) for (i) $NiWO_4$ and (j) $Ni_{0.875}Cu_{0.125}WO_4$. (k) Frequency dependent ε values measured by the impedance spectroscopy for $Ni_{1-x}Cu_xWO_4$ samples.

indicates that Φ is not much suppressed when varying *x*, a data consistent with the E_g and T_N results. Valence band spectra for all measured samples show states that die off close to the Fermi level, (E_F, see Fig. S8) indicating almost identical Φ to VBM level as a representative feature from the strongly correlated oxide with partially occupied *d*-bands with a high number of electrons.[15] This result strongly supports that the VBM band energy level in *p*-type $NiWO_4$ is pinned, and remains deeper than 5.56 eV associated with the rigid correlation strength with Cu substitution, while retaining the μ_H of other *p*-TCOs (Table S3).

Theoretical confirmation of a strongly correlated behaviour

To elucidate the underlying physics of the unprecedented charge transport behaviour, we performed DFT calculations. The band structures of the intrinsic $NiWO_4$ and $Ni_{1-x}Cu_xWO_4$ (x = 0.125) are shown in Figures 3a-d. Expectedly, without the explicit consideration of the electronic correlation in Ni *d* orbitals, E_g is considerably underestimated (~0.83 eV). With the direct inclusion of the Ni *d* Hubbard *U* (U_{Ni}) of 6 eV, in the form of DFT + *U*, the gap increases and becomes comparable to the experimental value of 3.0 eV. Compared to other systems with a *p*-*d* gap, where the Hubbard *U* does not contribute to the size of the gap, here it evidences the strong *d*-*d* character of the gap.[33,35] For the Cu-substituted case, to account for the higher occupation of Cu *d*-orbitals, we employed a Hubbard *U* (U_{Cu}) of 8 eV for Cu *d*,[25-27] which is slightly larger than the corresponding value for Ni. In between the *d*-*d* gap originating from Ni, the Cu *d* state is formed, which in turn slightly decreases the size of the E_g. This behaviour is consistent with the experimental optical absorption results in Fig. 2h. Our calculations show the importance of explicit inclusion of the Coulomb *U* in partially filled *d*-orbital systems, and unambiguously demonstrate the strongly correlated nature of the newly developed $Ni_{1-x}Cu_xWO_4$ *p*-type semiconductors. Figure 3e-h displays the corresponding partial density of states (PDOS) of $NiWO_4$ and $Ni_{1-x}Cu_xWO_4$ (x = 0.125). We can clearly observe the shift of the Ni and Cu *d* orbitals upon the inclusion of *U*. Figures S9 and S10 report the systematic evolution of the PDOS upon the inclusion of U_{Ni} and U_{Cu}, respectively. The PDOSs also confirm that the correlated electrons of localized *d* orbitals from Ni and Cu govern the low-energy physics of the system, and are the main origin for the almost invariant E_g and deep Φ value insensitive to the Cu impurity substitution concentration.

Polarizability estimation analysis relating with large polaronic conduction

Figure 3i and j shows the calculated charge density map near the VBM from E_F – 1 eV to E_F for $NiWO_4$ and $Ni_{0.875}Cu_{0.125}WO_4$, respectively. Thus, by replacing Ni with Cu the charge distribution changes both at the transition metal and the O sites. By comparing the PDOSs for the pristine and Cu-substituted cases in Fig. 3f and 3h, respectively, the hybridization of O *p* states, especially near the E_F, is enhanced, which is reflected in the charge density plot in Fig. 3i and 3j. This data, in turn, affects the overall polarizability of the system. Such an enhanced polarizability can be experimentally monitored by measuring the electrical permittivity (ε) (Fig. 3k). From impedance spectroscopy measurements, ε increases under wide frequency regime from 1 kHz to 1MHz upon increasing the Cu content from 0.00 to 0.20. (The possible origins for the increment on ε are discuss in section S12 in the ESI) The dimensionless electron-phonon coupling constant (α) is given by the following equation:[18]

$$\alpha = e^2\left(\frac{1}{\varepsilon_\infty} - \frac{1}{\varepsilon_0}\right)\sqrt{\frac{m}{2\omega_0}} \qquad (1)$$

where ε_0 and ε_∞ are the static and high-frequency dielectric constants, *m* is the effective mass, and ω_0 is the characteristic longitudinal optical phonon frequency. From equation (1), enhancing ε inevitably reduces α, thus it enlarges the polaron radius under long-range electron-phonon interactions, resulting in Fröhlich polaronic conduction.[17,18] This result, combined with the discussion reported in section S13 in the ESI, indicate that Cu substitution plays a critical role in μ_H enhancement by promoting the ionic polarizability in the system, while minimally influencing the electronic structure, since the correlation degree is preserved.

Material feasibility test in QD-LED and oxide *p/n* junction rectifier devices

Finally, we explored the use of *p*-type $Ni_{1-x}Cu_xWO_4$ as a HTL in opto-electronic devices. For QD-LED and *p/n* junction diode applications, $Ni_{1-x}Cu_xWO_4$ films of different thicknesses and functionality [30 nm as a conductive layer and 100 nm as a semiconducting layer (see Fig. S13)] were fabricated by RF magnetron sputtering of a $Ni_{1-x}Cu_xWO_4$ target (x = 0.185) with pure Ar and an Ar/O_2 mixture ($Ar:O_2$ = 2:1), respectively. Detailed film deposition conditions and device fabrication can be found in Methods. Figures 4a and 4b show the Raman and UV–vis transmittance spectra, respectively, of conductive and semiconducting $Ni_{0.815}Cu_{0.185}WO_4$ films deposited on glass substrates. As shown in Figs. 4a, the characteristic W-O A_g Raman peaks of sputtered samples are slightly blue-shifted and broadened (460, 560 and 960 cm^{-1}, see the arrows in Fig. 4a) compared to those of the bulk samples (420, 550 and 900 cm^{-1}, Fig. S4), due to the amorphous phase (see the inset XRD in Fig. 4a).[28] However, the direct E_g's of all samples are almost identical to those measured for the bulk (Fig. 4b) corroboration the quality of the sputtered thin-films and reproducibility of Cu incorporation in $NiWO_4$. The slight reduction in E_g values in thin films are mainly attributed to the tail states formation originating from the amorphous nature.[36,37] The transmittance in the visible for the most transparent film (100 nm thick, Ar/O_2 deposited) is ~96%, demonstrating its transparent nature as a *p*-type TCO film.

Figure S14a reports the schematic representation and the high-resolution cross-sectional transmission electron microscopy (HR-TEM) image of the QD-LED device with a 30 nm thick $Ni_{0.815}Cu_{0.185}WO_4$ HTL deposited under Ar-only working pressure condition to enhance conductivity (refer to section S14 for discussion). Note no additional blocking layers are used for balancing charge injection from the electrodes.[38-43] The QD-LED energy band diagram in Fig. S14b indicates that the deep-lying VBM of $Ni_{0.815}Cu_{0.185}WO_4$ with a wide E_g is beneficial not only for

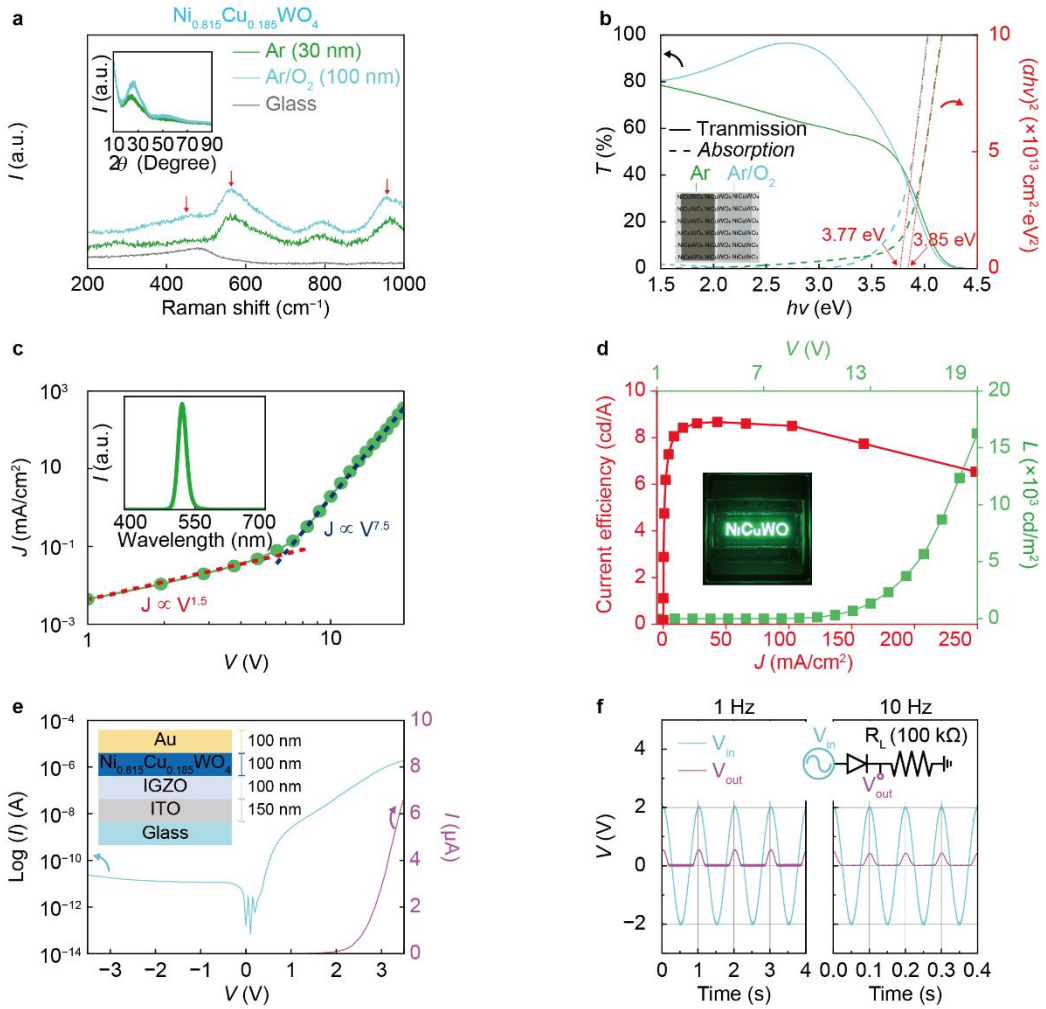

Figure 4. QD-LED and oxide *p/n* rectifier adopting $Ni_{1-x}Cu_xWO_4$. (a) Raman and (b) transmittance spectra from RF-sputter deposited $Ni_{0.815}Cu_{0.185}WO_4$ thin films on glass substrate fabricated in Ar only (30 nm, for use in QD-LED) and Ar/O_2 (100 nm, for use in a rectifier diode) conditions. The XRD results and photo of the $Ni_{0.815}Cu_{0.185}WO_4$ thin-film are displayed in the inset of Fig. 4a and 4b, respectively. (c) Current density (*J*) – voltage (*V*), (d) current efficiency (left axis) – *J*, and luminescence (*L* in right axis) – *V* curves of a QD-LED utilizing $Ni_{0.815}Cu_{0.185}WO_4$ as the HTL. Electroluminescence (EL) spectrum and photograph of green emission are shown in the inset of Fig. 4c and 4d, respectively. (e) Current (*I*) – *V* characteristic of a *p*-$Ni_{0.815}Cu_{0.185}WO_4$/*n*-IGZO junction diode. The oxide-based *p/n* diode schematic is illustrated in the inset of Fig. 4e. (f) AC to DC rectifying behaviour using a 2V peak-to-peak sinusoidal input voltage (V_{in}) and the corresponding output voltage (V_{out}) signal. The circuitry configuration is schematically shown in the inset of Fig. 4f.

lowering the hole injection barrier, but also for increasing the electron-blocking barrier between the HTL and CdSe-based QD compared to other HTL materials.[38-43] Such an advantage is reflected by the device performance. Fig. 4c shows the current density versus applied voltage (*J-V*) characteristics for the device, evidencing an ohmic conduction region ($J \propto V^{1.5}$) up to 6.5 V and a clear trap-limited conduction region ($J \propto V^{7.5}$) in the voltage regime higher than 6.5 V. Based on the ohmic conduction behaviour below 6.5 V, the $Ni_{0.8}Cu_{0.2}WO_4$ HTL serves as a simple charge conductor following Ohm's law.[39,41] In the trap-limited conduction regime above 6.5 V, light emission occurs by electron-hole recombination in the QDs layer acting as trap centres.[41,43] In the case of current-driven light-emitting diodes, the position of the electron-hole recombination zone is very important to prevent additional emission compromising colour purity.[38,43] Fig. 4c-inset shows only a single symmetric electroluminescence (EL) emission peak at 523 nm with a narrow full-width at half-maximum (FWHM) of 24.89 nm, demonstrating that balanced charge recombination only occurs in the QDs even without any additional blocking layers.[38-43] Our QD-LED shows a maximum luminescence (*L*) and current efficiency (η) of 16258 cd/m² and 8.67 cd/A, respectively (Fig. 4d), which are greater than those of green CdSe QD devices with similar structure (Table S4). Since the roll-off behaviour of η is relatively small compared to other CdSe-based QD-LEDs, the significantly improvement device performance is attributed to enhanced hole-electron charge balance.[38-43]

Additionally, we broaden applicability of our *p*-type TCO to circuitry by fabricating an oxide-based *p/n* junction rectifier. As displayed in Figure 4e-inset, a 100 nm-thick *p*-$Ni_{0.815}Cu_{0.185}WO_4$ layer is deposited on an *n*-type IGZO film of the same thickness, resulting in a transparent oxide *p/n* junction. The *I-V*

characteristic in Fig. 4e demonstrates prominent rectifying behaviour with a high on/off current ratio of 5.6×10^4 compared to other oxide diodes (Table S5). Considering that *n*-IGZO and *p*-$Ni_{0.815}Cu_{0.185}WO_4$ are both amorphous with an identical thickness, such a good switching behaviour originates from their well-balanced charge transport characteristics under a large built-in potential (Fig. S15). Next, taking advantage of the good diode characteristics, an AC to DC converting circuit is assembled with a 100 k Ω load resistor (R_L). As shown in Figure 4f, when a sinusoidal input signal (V_{in}) is applied with a -2 ~ +2 V peak-to-peak amplitude, AC to DC signal rectification can be measured up to 10 Hz without delaying. These results demonstrate the applicability of this new material for practical transparent device applications.

Conclusions

We demonstrated the underlying physics of a new hole transparent conductor, $Ni_{1-x}Cu_xWO_4$, with performance comparable to those from the other *p*-TCOs, while exhibiting the deepest Φ value. Structural, compositional, and vibrational studies revealed that Cu substitutes Ni, resulting in $Ni_{1-x}Cu_xWO_4$ solid solutions up to x = 0.20. Electrical measurements confirm that the μ_H of $NiWO_4$ significantly increases by Cu incorporation, even leading to the emergence of band-like large polaronic conduction behaviour. The E_g, T_N, and Φ values of $Ni_{1-x}Cu_xWO_4$ minimally change with the Cu content, supporting the sustained electron correlation strength in $NiWO_4$ regardless of the Cu content. DFT calculations and impedance spectroscopy measurements demonstrate that the enhanced polarizability plays a crucial role in the emergence of delocalized hole transport along a rigid deep-lying VBM band down to 5.77 eV. Finally, we utilized $Ni_{1-x}Cu_xWO_4$ films as the HTL and *p*-type layer in QD-LED and rectifier devices, demonstrating the use of this *p*-type TCO in practical applications. Our results offer a novel strategy for expanding the functionality of strongly correlated materials and *p*-type TCO design.

Author contributions

K.L., K.H.L., M.S.O., and A.F.: Conceptualization, Resources, Supervision, Validation, Funding acquisition, Project administration, Writing-original draft, Writing-review & editing. S.Y.L., I.K., and H.J.K.: Data curation, Formal analysis, Investigation, Methodology, Validation, Visualization. S.S., J.H.K., S.Y., J.B., K.W.P, C.J.H., H.M.K., H.Y., B.J.K., and S.I.: Data curation, Investigation, Resources, Software, Validation.

Conflicts of interest

There are no conflicts to declare.

Data availability

The data supporting this article have been included as part of the ESI.

Acknowledgements

This work was supported by the National Research Foundation of Korea (NRF) grant funded by the Korea government (MSIT) (No. RS-2024-00401881, No. 2022R1A2C2005210, and No. RS-2024-00411892). It was also financially supported by the Ministry of Trade, Industry and Energy (MOTIE) and Korea Planning & Evaluation Institute of Industrial Technology (KEIT) through the Industry Technology R&D Program (20016332). It was partly supported by Samsung Research Funding & Incubation Center of Samsung Electronics under Project Number SRFC-MA1902-03. AF acknowledges NSF (award # 2223922) for support.

References

1 S. M. Sze & Kwok. K. Ng, *Physics of Semiconductor Devices 3rd ed.* (John Wiley & Sons, 2007).
2 S. M. Kang & Y. Leblebici, *CMOS Digital Integrated Circuits: Analysis and Design 3rd ed.* (McGraw-Hill, 2003).
3 K. Nomura, *J. Inf. Disp.*, 2021, **22**, 211.
4 A. M. Ionescu & H. Riel, *Nature*, 2011, **479**, 329.
5 K. Fai & J. Shan, *Nat. Photonics*, 2016, **10**, 216.
6 S. O. Kasap, *Optoelectronics and Photonics: Principles and Practices 2nd ed.* (Pearson Education, 2013).
7 A. Polman, M. Knight, E. C. Garnett, B. Ehrler, and W. C. Sinke, *Science*, 2016, **352**, aad4424.
8 X. Yu, T. J. Marks, and A. Facchetti, *Nat. Mater.*, 2016, **15**, 383.
9 D. S. Ginley, H. Hosono, and D. C. Paine, *Handbook of Transparent Conductors.* (Springer, 2010).
10 J. E. Medvedeva, D. B. Buchholz, and R. P. H. Chang, *Adv. Electon. Mater.*, 2017, **3**, 1700082.
11 A. Murat, A. Adler, T. O. Mason, and J. E. Medvedeva, *J. Am. Chem. Soc.*, 2013, **135**, 5685-5692.
12 B. Wang *et al. Nat. Commun.*, 2020, **11**, 2405.
13 J. Kim, M. Jeong, B. Kim, and J. Jang, *IEEE Elec. Dev. Lett.*, 2022, **43**, 1471.
14 Z. Wang, P. K. Nayak, J. A. Caraveo-Frescas, and H. N. Alshareef, *Adv. Mater.*, 2016, **28**, 3831.
15 M. T. Greiner *et al. Nat. Mater.*, 2012, **11**, 76.
16 P. A. Cox, *The Electronic Structure and Chemistry of Solids* (Oxford University Press, 1987).
17 I. G. Austin and N. F. Mott, *Adv. Phys.*, 2001, **50**, 757.
18 C. Franchini, M. Reticcioli, M. Setvin, U. Diebold, *Nat. Rev. Mater.*, 2021, **6**, 560.
19 L. Zhang *et al. Nat. Mater.*, 2016, **15**, 204.
20 K. H. L. Zhang *et al. Adv. Mater.*, 2015, **27**, 5191.
21 S. G. Park *et al. Inorg. Chem. Front.*, 2020, **7**, 853.
22 G. Kresse and D. Joubert, *Phys. Rev. B*, 1999, **59**, 1758.
23 G. Kresse and J. Furthmüller, *Phys. Rev. B*, 1996, **54**, 11169.
24 J. P. Perdew, K. Burke, M. Ernzerhof, *Phys. Rev. Lett.*, 1996, **77**, 3865.
25 S. L. Dudarev, G. A. Botton, S. Y. Savrasov, C. J. Humphreys, and A. P. Sutton, *Phys. Rev. B*, 1998, **57**, 1505.
26 H. Eskes, L. H. Tjeng, and G. A. Sawatzky, *Phys. Rev. B*, 1990, **41**, 288.
27 R. Tesch and P. M. Kowalski, *Phys. Rev. B*, 2022, **105**, 195153.
28 A. Kuzmin, J. Purans, R. Kalendarev, *Ferroelectrics*, 2001, **258**, 21.
29 J. H. Ryu *et al. Scripta Materialia*, 2020, **182**, 6.
30 C. C. Wang, S. A. Akbar, W. Chen, and V. D. Patton, *J. Mater. Sci.*, 1995, **30**, 1627.
31 T. Sakanoue and H. Sirringhaus, *Nat. Mater.*, 2010, **9**, 736.
32 M. A. Pronsnikov, V. Y. Davydov, A. N. Smirnov, M. P. Volkov, and R. V. Pisarev, *Phys. Rev. B*, 2017, **96**, 014428.

33 M. Imada, A. Fujinori, and Y. Tokura, *Rev. Mod. Phys.*, 1998, **70**, 1039.
34 K. Lee, S. W. Kim, Y. Toda, S. Matsuishi, H. Hosono, *Nature*, 2013, **494**, 336.
35 J. E. Medvedeva, V. I. Anisimov, O. N. Mryasov, A. J. Freeman, *J. Phys.: Condens. Matter.*, 2022, **14**, 4533.
36 T. Kamiya and H. Hosono, *NPG Asia Mater.*, 2010, **2**, 15.
37 T. Kamiya, K. Nomura, and H. Hosono, *Phys. Status Solidi A*, 2009, **206**, 860.
38 X. Yang *et al. Nano Energy*, 2018, **46**, 229.
39 Y. Jiang *et al. ACS Appl. Mater. Interfaces*, 2019, **11**, 11119.
40 Y. Zhang and L. Zhao, *J. Mater. Res.*, 2019, **34**, 2757.
41 J. M. Caruge, J. E. Halpert, V. Wood, V. Bulović, M. G. Bawendi, *Nat. Photonics*, 2008, **2**, 247.
42 W. Ji *et al. ACS Photonics*, 2017, **4**, 1271.
43 H. Y. Kim *et al. Adv. Funct. Mater.*, 2016, **26**, 3454.H. Eskes, L. H. Tjeng, and G. A. Sawatzky, *Phys. Rev. B*, 1990, **41**, 288.

Data availability

The data supporting this article have been included as part of the ESI.